Journal of Applied Fluid Mechanics, Vol. 11, No. 3, pp. 679-688, 2018.
Available online at www.jafmonline.net, ISSN 1735-3572, EISSN 1735-3645.
DOI: 10.29252/jafm.11.03.28344

Numerical Analysis of the Effects of Riblets on Drag Reduction of a Flat Plate

A. Heidarian[1], H. Ghassemi[2†] and P. Liu[3]

[1]*Department of Marine Engineering, Persian Gulf University, Bushehr, Iran*
[2]*Department of Maritime Engineering, Amirkabir University of Technology, Tehran, Iran.*
[3] *Australian Maritime College, University of Tasmania, Locked bag 1395, Launeston, TAS 7250, Australia and International School of Ocean Sicence and Engineering, Harbin Institute of Technology, Weihai, 264200, China.*

†*Corresponding Author Email: gasemi@aut.ac.ir*

(Received August 25, 2017; accepted December 12, 2017)

ABSTRACT

In recent years, marine transportation as well as land and air transportation has become in the centre of attention. There has been an attempt to reduce the drag exerted on vessels by various methods, such as rough surfaces and base bleed. Study of the high-speed seawater animals like sharks and dolphins has triggered the use of riblets on the hull of marine vessels. The use of riblet is easy among various methods of skin friction drag reduction. For this reason, there is an interest for construction and optimization of riblet as an efficient and economical way. In this research, the shark's skin was modeled for the first time in *ANSYS CFX* using Computational Fluid Dynamics, through analyzing the effects of riblet on a submerged flat plate. Different types of riblet based on height and space between micro channels were studied, and then a comparison between a riblet-covered plate and a smooth plate in various velocities were performed. It was found that by selecting the most appropriate type of riblet, 11 % drag reduction can be attained. Then, by comparing different types of riblets, the best type for drag reduction was selected. Furthermore, the obtained results were compared with the available experimental data.

Keywords: Drag reduction; Flat plate; Riblet; Micro channels.

1. INTRODUCTION

There are various ways in nature to reduce drag force in fluid flow, such as the evidences in the movements of fish, sharks and dolphins (Hoyt, 1975). The compliant skin of dolphins has been studied for drag reduction capabilities, and showed to be useful by responding to the pressure fluctuations across the surface (Davies and Carpenter, 1997a). Though early studies showed dramatic drag reduction benefits, later studies have only been able to confirm 7 % drag reduction (Choi *et al*., 1997).

Determining the optimal riblet specifications for maximum drag reduction is significant. Different geometries, configurations and materials for riblet and various fluids and flow regimes have been examined through experiments (W. D. Bechert, Bruse, and Hage, 2000)

Riblets are beneficial for drag reduction of objects where the drag is caused by turbulent flow, thus suitable for the long objects with fairly flat edges. Riblets are not effective on objects with pressure drag as their dominant drag force (Dean and Bhushan, 2010). Cases where riblets were applied in practice include the use of saw tooth riblets manufactured by 3M Company on an Olympic boat and an American sailing yacht in mid 1980s, which showed good effect. It was also applied on test planes, though never used on commercial flights (Brian Dean, 2012). While good results were obtained in testing, it was calculated that only 3% drag reduction can be obtained for a commercial plane considering the limitations in the areas where riblets can be implemented (D. W. Bechert, Bruse, Hage, Van Der Hoeven, and Hoppe, 1997). So far, riblets have commercially applied in racing swimsuits specifically for drag reduction purposes, which has been successfully used in Olympics by an American athlete. It is reported that by wearing these swimsuits drag can be reduced by 4 % for men and 3 % for women (Krieger, 2004).

Geometry of riblets includes blade, saw tooth, scalloped, and bullnose with continuous and segmented configurations (aligned and staggered). Typical geometries of saw tooth, scalloped and blade riblets are shown in Fig. 1 (Zhao, Tian, Wang, and Jin, 2014).

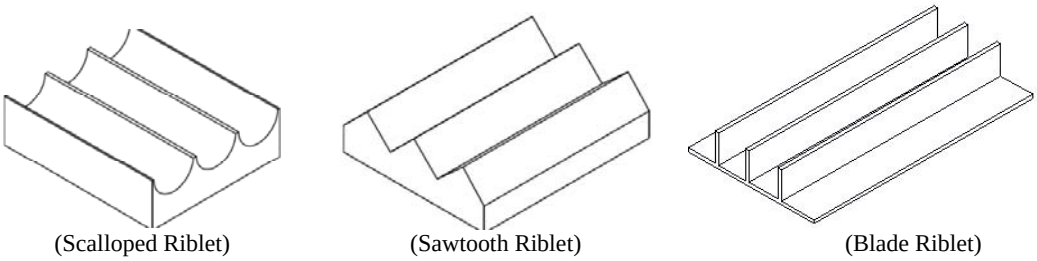

Fig. 1. Different types of riblet (Bixler and Bhushan, 2012).

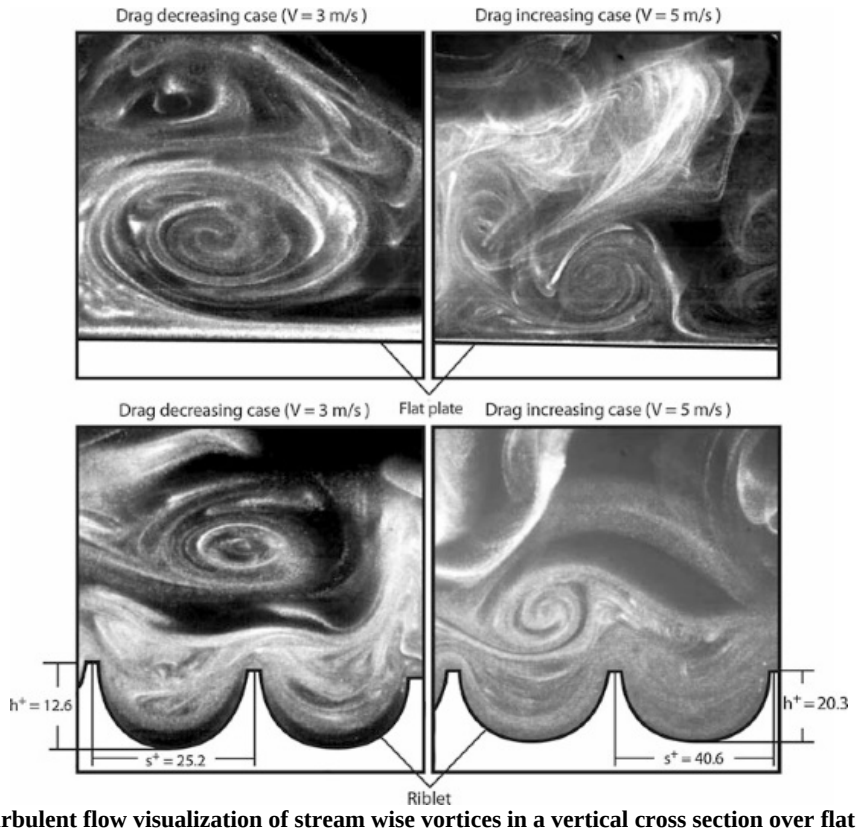

Fig. 2. Turbulent flow visualization of stream wise vortices in a vertical cross section over flat plate and riblet surfaces (Lee and Lee, 2001).

When an object moves in a fluid, the drag is due to the pressure drag and friction drag. Pressure drag is caused by the pressure differences between the back and front of the object, and friction drag is a result of both the interactions between the fluid and the object surface and attractions between the molecules of the fluid (Fu, Yuan, and Bai, 2017). The drag on an object is representative of the energy needed for momentum transfer between the fluid and the object. This transfer of momentum is used to create a velocity gradient from the surface, where the velocity is zero based on the no slip wall condition, to the undisturbed fluid above the surface (Fuaad, Baig, and Ahmad, 2016).

In turbulent conditions, where the fluid molecules move in nonparallel directions and thus cross flow velocities exist between the molecules, a noticeable increase in momentum transfer will occur. This increase is of high significance, because any momentum transfer parallel to the object surface will increase the drag force (Brown and Roshko, 1974).

Riblets, the small pieces covering the surface of the object are utilized to reduce the increased drag in turbulent flow by decreasing the shear stress and momentum transfer (Carman *et al*., 2006). This is possible by the elevating the vortices above the surface and preventing the cross-stream movement of the streamwise vortices in the viscous sublayer (Bixler and Bhushan, 2012) the captured phenomenon in a vertical cross section over flat plate and riblet surfaces are shown in Fig. 2.

The use of riblet for the purpose of drag reduction does not seem obvious at the beginning, because it increases the total wetted area, thus increases the drag due to the rise in the shear stress (Matin, Merah, and Ibrahim, 2016).

But, another mechanism appears here, which is the lifting of the vortices by the riblets. What happens is that riblets shift the formed vortices towards the

riblet tips and fluid with lower velocity will flow between the tips (Shelley, Smith, Hibbins, Sambles, and Horsley, 2016). Therefore, the interaction of vortices is only with the small surface of the tips and high shear stress acting on this small area whereas the large area between the tips experiences a slight shear stress caused by the low velocity flow. When the vortices are kept above the tips, the fluctuations of the cross stream velocity between the riblets are much lower than that above a flat plate. Therefore, the shear stress and momentum transfer are lower near a riblet covered surface, which reduce the effect of increased area due to the riblets (Goldstein, Handler, and Sirovich, 1995).

2. RIBLET OPTIMIZATION

Important parameters for a riblet include spacing (*s*), height (*h*), and thickness (*t*), which are essential parameters to achieve the best drag reduction. Variation of these parameters leads to changes in the maximum drag reduction. In this study, different ratios of height to distance (*h/s*) for riblets were investigated to choose the best type. Based on the experimental result of the work done by NASA and BMW company on a hydrofoil boat using the riblet of *3M* Company, the efficient type of riblet for drag reduction is with a dimension of $h/s = 0.5$ for saw tooth riblets (Krieger, 2004).

To characterize induced vortices and riblet structures, understanding the dimensions is essential. Dimensions of the turbulent flow structures vary by the change of the flow properties. Therefore, non-dimensional length values have been used for better comparison of the studies in various conditions of the flow (Shelley, Smith, Hibbins, Sambles and Horsley, 2016). Here, all length scales were multiplied by $\frac{V_\tau}{\nu}$ and marked by +. For instance, non-dimensional riblet spacing s^+ is given by

$$s^+ = \frac{sV_\tau}{\nu} \tag{1}$$

Where s is the dimensional riblet spacing, ν is the kinematic viscosity

$$V_\tau = \left(\frac{\tau_0}{\rho}\right)^{1/2} \tag{2}$$

Represents the wall stress velocity and ρ is the fluid density. For pipe flow

$$\tau_0 = 0.03955\nu^{1/4}\rho V^{7/4}D^{-1/4} \tag{3}$$

τ_0 Is the wall shear stress, V is the average flow velocity and D is the hydraulic diameter, calculated for flow in rectangular pipes as

$$D = \frac{4A}{C} \tag{4}$$

Where A is the cross sectional area and c is the wetted perimeter

Riblets performance changes with the variation of the essential parameters like *h* and *s*. For example, experimental data using a ratio of $h/s = 0.86$ showed 9 % drag reduction, while the use of $h/s = 0.7$ resulted in 6.5 % drag reduction (Bhushan, 2012).

According to the experimental data by (Bixler and Bhushan, 2012), the maximum drag reduction occurred for $h/s = 0.5$ in saw tooth riblets. Based on this data, the same ratio of h/s was chosen in the present numerical simulation to observe the velocity and pressure contours and to investigate the performance of riblets in reducing drag force.

2.1. Governing Equations

Principle of mass conservation, also known as the continuity equation, is a significant equation, which could be applied to every domain of current regardless of any simplifying assumptions (M and A, 1984). This principle states that for any system involving matter and energy transfer, the mass of the system remains constant over time. The short form of the equation gives

$$\frac{\partial \rho}{\partial t} + \frac{\partial(\rho u_i)}{\partial x_i} = 0 \tag{5}$$

By taking incompressibility of fluid into consideration, the continuity equation would be:

$$\frac{\partial u_i}{\partial x_i} = \frac{\partial u}{\partial x} + \frac{\partial v}{\partial y} + \frac{\partial w}{\partial z} = 0 \tag{6}$$

According to the Newton's law of viscosity, a shear stress exerted by a force parallel to the surface, is proportional to the rate of deformation or strain rate. Such a shear stress occurs if the flow has a velocity gradient. In fact, Navies–Stokes equations indicate conservation of momentum, mathematically. The aforementioned equation for an incompressible fluid is as follows:

$$\frac{\partial(\rho u_i)}{\partial t} + \frac{\partial}{\partial x_j}(\rho u_i u_j) = -\frac{\partial p}{\partial x_i} + \left[\mu\left(\frac{\partial u_i}{\partial x_j} + \frac{\partial u_j}{\partial x_i}\right)\right] + \rho g_i \tag{7}$$

2.2. Turbulence

In the case of modeling the fluid flow, all governing equations are needed. Besides, when dealing with high Reynolds numbers, that is turbulent flow, time and space oscillations are two characteristics of the flow.

Usually, modeling these flows sounds impossible in engineering applications because oscillations happen on small scales and have high frequencies.

Perhaps, in theory, these could be modeled for simple geometries and for low Reynolds numbers by using direct numerical simulation (*DNS*). Obtaining the solution of the original Navies–Stokes equations, in the case of oscillations on small scales, and high frequencies does not seem to be economically efficient at all.

3. NUMERICAL ANALYSIS

Numerical calculations were performed using the commercial computational fluid dynamics code

ANSYS CFX 14.5 (*ANSYS CFX-Solver Theory Guide*, 2011) The geometry is shown in Fig. 3. In this simulation, a flat plate without and with riblets, of different types and dimensions of riblet was placed in the fluid flow at various velocities. There is a possibility to use five different turbulence models in ANSYS CFX including *k–ε, k– ω, SST, BSL* and *SSG*, each containing different hypotheses and equations describing the models.

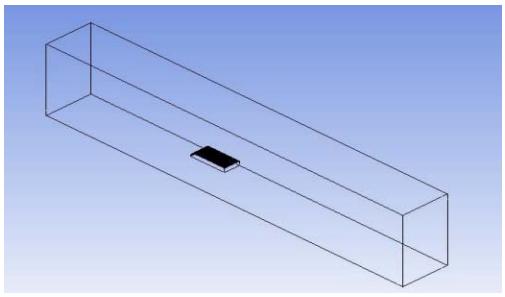

Fig. 3. Flat plate in rectangular duct.

RANS was used in our simulations using steady-state with the shear stress transport (*SST*) turbulence model. The *SST* model applies a *k–ω* based model formulation in proximity of the wall and the *k–ε* model for the remaining part of the flow field.

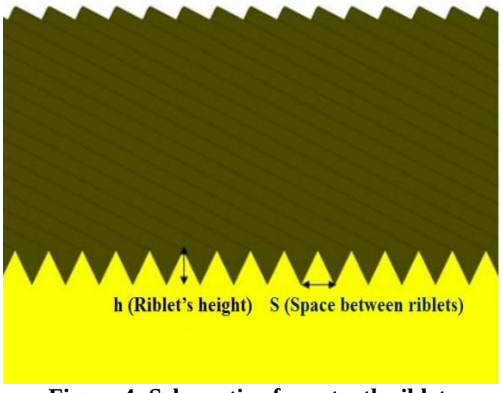

Figure 4: Schematic of saw tooth riblets

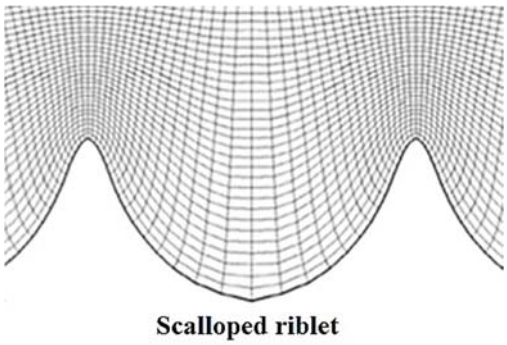

Fig. 5. Schematic of scalloped riblets.

Two different types of riblets, namely saw tooth and scalloped were used in the simulations, of which the schematics are given in Figs. 4 and 5, respectively. Scalloped riblets are most commonly defined by their h/s ratio, but test shapes have been varied between research groups. Although they are similar in their basic shapes, a standard scalloped profile has not yet been established. In general, any concave shape may be referred to as scalloped. Comparison of the data from saw tooth and scalloped riblet optimizations enables a generalization of comparable shapes. The desirable tip of the riblet is thin and sharp, however good results have been produced by scalloped riblets with measurable tip thicknesses.

3.1. Meshing

Five different meshes representing coarse (447,401 nodes), medium (1,053,680 nodes), fine (2,238,573), very fine (4,464,312 nodes) and extreme fine (6,464,312) were examined to select the best mesh for the riblets based on the maximum y^+ and drag coefficient. As it can be seen in Table 1, the drag coefficient changes from the coarse mesh to the extreme fine mesh, where an acceptable maximum $y^+ = 34$ is achieved. This value assures that the boundary layer can be fairly well resolved on this mesh. To check the independence of the mesh, finer meshes of 4,464,312 and 6,464,312 nodes were also examined and no variation has been obtained for the drag coefficient. Inflation was considered around the flat plate and the size of mesh was changed. By 2.3 million nodes the drag coefficient reached to 0.0179 and after introducing inflation by the first layer height of 5e-4, about 4 million elements were acquired and drag coefficient was reached to 0.0.0179702 (about 0.5 percent difference). Then the height of the first layer was changed to 1e-4 and achieved to about 6 million elements and drag coefficient was led to 0.0180. Therefore, the fine mesh was selected for the simulations, which is shown in Fig. 6.

4. RESULTS AND DISCUSSION

4.1. Drag Coefficient

Drag reduction of different types of riblet depends on the type and dimensions of riblets. For this reason, six different ratios of h/s and two types of riblets were simulated and their drag and lift coefficients were captured based on *h/s* ratio and Reynolds number.

Plots in Fig. 7 show numerically simulated flow over a plate without and with riblet on top of the surface. Values of drag reduction are based on the size of the riblet. The diagram reveals that the drag coefficient of the riblet plate is less than a simple plate.

The largest drag reduction occurred for the ratio of approximately *h/s* = 0.5 for saw tooth riblets and approximately *h/s* = 0.7 for scalloped riblets. This is the most optimal riblet size and the best choice for maximum drag reduction, which is also verified through experimental data. According to the chart, by reducing the ratio of the height to the distance between riblets, the drag coefficient is increased. Results show optimization data for scalloped riblets. A maximum drag reduction of 5.1 % for scalloped riblets with *h/s* = 0.7, and 11 % for saw tooth riblets with *h/s* = 0.5 have been obtained.

The effects of different h/s ratios of riblets on the lift coefficient have been investigated and the results are shown in Fig. 8. As it can be seen Figs. 7 and 8, the increase in lift coefficient by using riblets eventually leads to the reduction in drag coefficient.

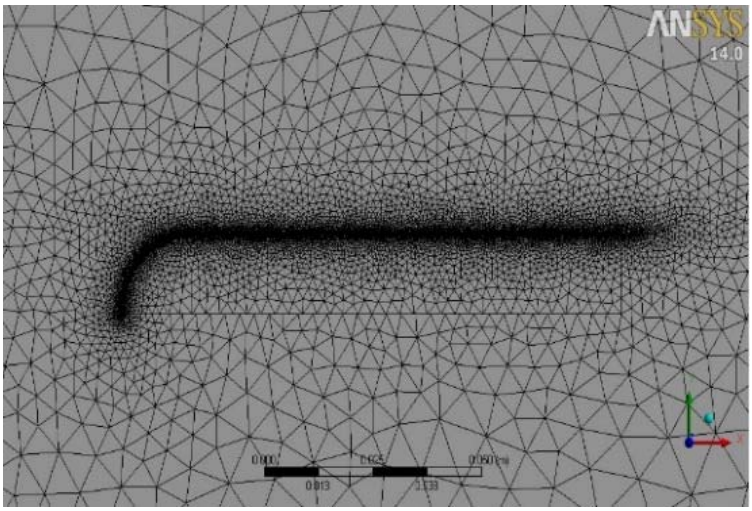

Fig. 6. Meshing around riblets on top of plate's surface.

Table 1 Different meshes examined for the riblets

Mesh	Nodes	Max y^+	Drag coefficient
Coarse	447,401	180	0.131
Medium	1,053,680	83	0.0806
Fine	2,238,573	63	0.0179
Very Fine	4,464,312	47	0.0179702
Extreme Fine	6,464,312	34	0.0180

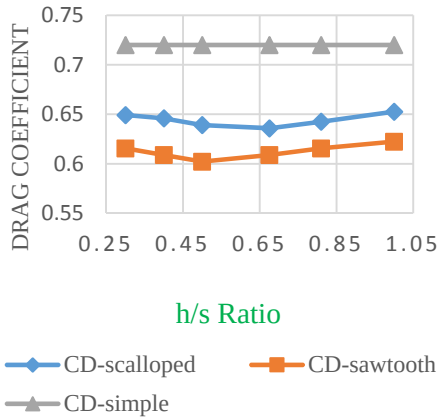

Fig. 7. Drag coefficient of different types of riblets compared with simple flat plate based on h/s ratio.

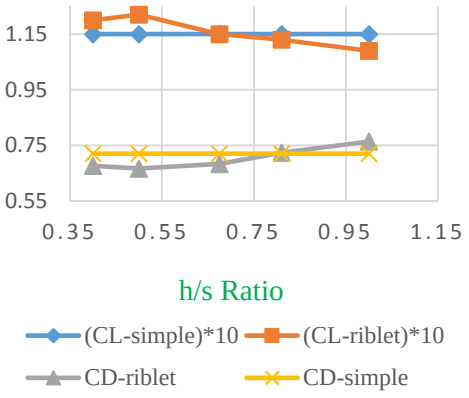

Fig. 8. Lift and drag coefficients of riblets compared with simple flat plate based on h/s ratio.

The graph in Fig. 9 compares the values of drag coefficient based on Reynolds number for the saw tooth riblets at *h/s* = 0.5 and simple flat plate. It shows that by increasing the speed, drag coefficient is reduced and the maximum amount of drag reduction of riblet flat plate is 11 % for the saw tooth riblets.

Figure 10 represents the pressure around the riblet plate and simple flat plate. Pressure contours are captured at 30 m/s for two different types of riblets having different dimensions. Pressure distribution in the simple plate indicates that a large area of plate is at high pressure indicating that the plate is receiving a higher drag force.

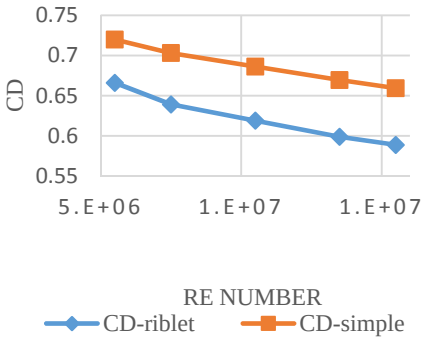

Fig. 9. Drag reduction of saw tooth riblets at h/s=0.5 compared with simple flat plate based on Reynolds number.

4.2. Pressure Contours

In the flat plate having applied riblets on the surface, the pressure at the tip is less than the one in a simple plate. Less pressure at the tip indicates that the force of the fluid applied on the flat plate is reduced. Pressure distribution in the simple plate indicated that large areas of plate are at high pressure and hence the plate receives higher force. However, pressure distribution in the simple flat plate is uniform and upper and lower surfaces have approximately the same pressure. As a result, lift force in this type is lower than that in riblet plate. In saw tooth riblets with *h/s*=0.5, the upper surface has lower pressure than the lower surface and this is the reason why this type of riblet has maximum lift extraction compared to other types of riblet. As h/s ratio increases, the lift extraction decreases.

Pressure distribution in riblet flat plate with *h/s*=162/324 shows that the pressure difference is higher than the ones for other types of riblets. More pressure gradient on the plate indicates higher lift force on flat plate. Figure 11 shows pressure distribution from the top view of flat plates in the simple plate and different riblet plates with various geometries. In the simple flat plate, pressure dropped in major parts of plate and this drop causes the separation of the fluid and velocity increases. In scalloped riblet types, the decrease in pressure at the back of flat plate is more than that of the saw tooth riblets.

When the pressure of flat plate is increased, it begins to move easily, because hydrodynamics pressure helps it to lift, thus received lower hydrodynamics pressure, but in another sizes of riblet, no auxiliary force exists and needs a higher energy to move. Thus a bigger engine is needed leading to an increased cost of production. In riblet flat plate, stagnation point goes to a lower position and therefore less pressure is inserted to sensitive areas of flat plate and pressure decreases at the leading edge.

4.3. Velocity Contour of Saw Tooth Riblets

Velocity contours of riblet plate and simple flat plate are shown in Fig. 12. Based on the figure, the separation on riblet flat plate is delayed compared to the simple flat plate. It means that major parts of flat plate have smaller pressure and force due to the reduction of fluid separation and lift force is increased at similar velocities. Bottom of riblet flat plate has smaller velocity and thus higher pressure compared to the simple flat plate.

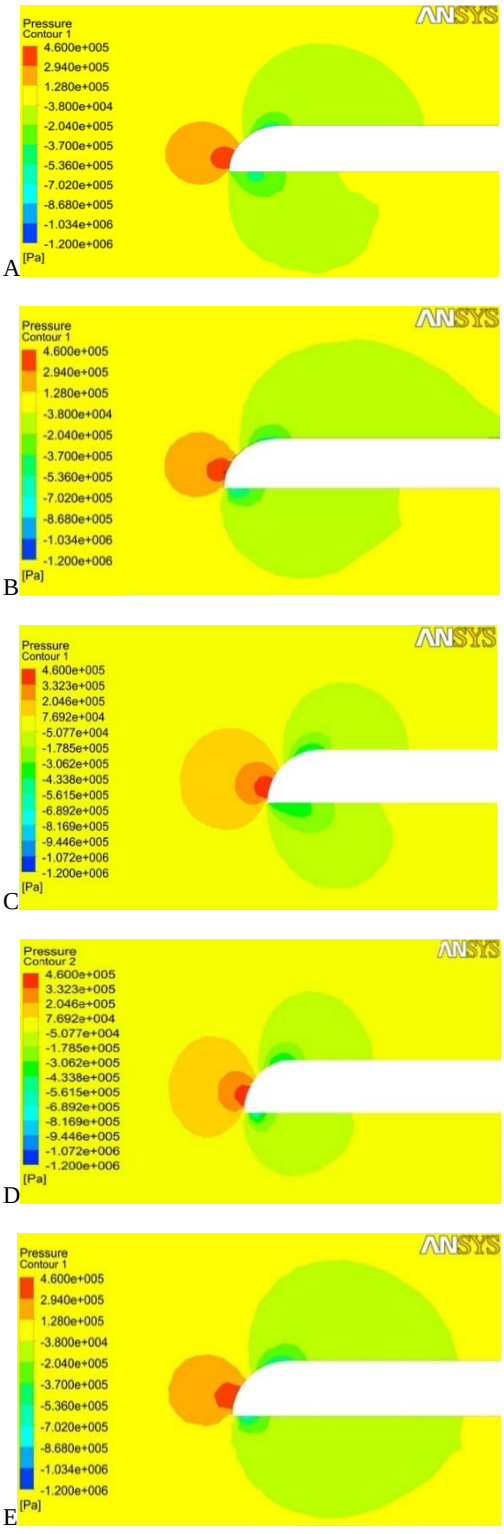

Fig. 10. Pressure contours for different h/s ratios at a velocity 30 m/s. A: 162/162 saw tooth riblet, B: 162/324 saw tooth riblet, C:162/162 scalloped riblet, D:162/240 scalloped riblet, E: Simple flat plate.

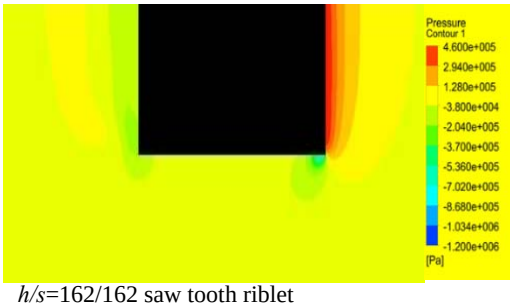

h/s=162/162 saw tooth riblet

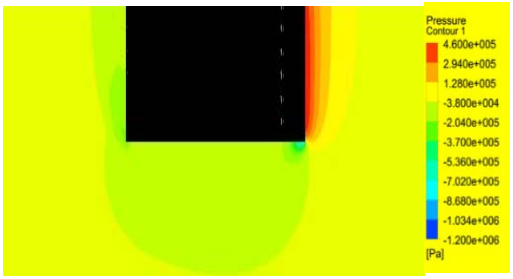

h/s=162/162 scalloped riblet

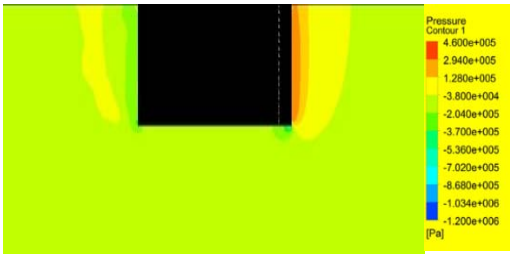

h/s=162/324 saw tooth riblet

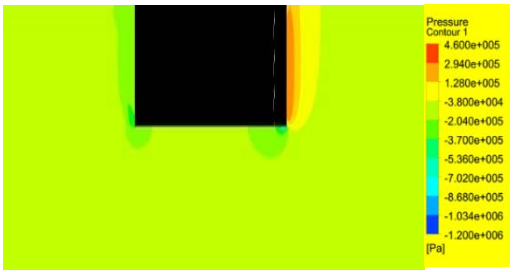

h/s=162/240 scalloped riblet

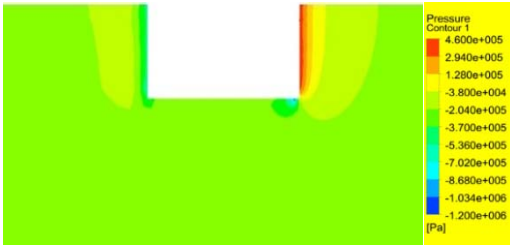

Simple flat plate without riblet

Fig. 11. Pressure status at leading edge of the flat plate (top view).

4.4. Vortices Status Behind the Flat Plate

Eddy viscosity- a function of the flow- is greater for more turbulent flows. Momentum transfer by eddies in turbulent flows gives rise to internal fluid friction. Separation on flat plates sometimes occurs around the leading edge giving rise to a short bubble. It can be dangerous because it usually occurs toward the trailing edge so the flow cannot be reattached. Then, the separated region merges with the wake and may cause serious structural failures.

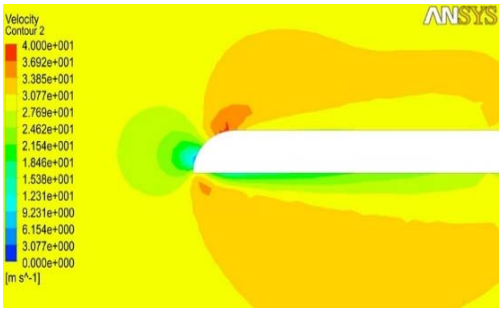

A

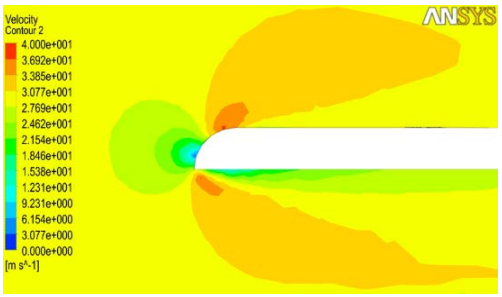

B

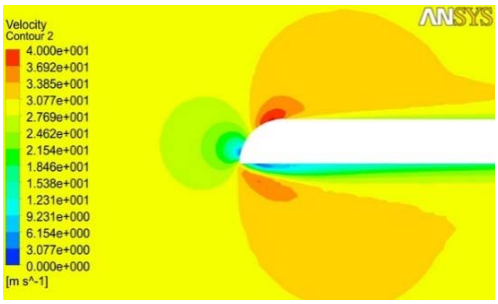

C

Fig. 12. Velocity contour of, A: Simple flat plate, B: saw tooth riblet, C:scalloped riblet.

Figure 13 shows the vortices behind flat plate without and with riblet having different dimensions. Both types of flat plate simulated at the same condition, but final velocities in riblet types are higher than simple flat plate. This increase in speed is due to the fluid flowing in micro-channel eliminating cross-speed component. Therefore, all the flow's energy spends only in one direction increasing fluid turbulence.

Using micro-riblet film causes the flow to converge. Higher energy and momentum of the turbulent flow compared to the laminar flow can eliminate separation and the flow may reattach. A short bubble may not cause much consequence.

Table 2 Maximum drag reduction with different types of riblet in different fluids that were obtained from experiments and present study

Fluid	Riblet Design	Maximum Drag Reduction	Ref
Water	Sawtooth	6%	(Walsh & Lindemann, 1984)
Water	Sawtooth	9%	(Shephard, 1994)
Water	Sawtooth	13%	(W. D. Bechert *et al*., 2000)
Oil	Blade Riblet	9.9%	(D. Bechert *et al*., 1997)
Air	Sawtooth	8%	(Davies and Carpenter, 1997b)
Air	Sawtooth Riblet	8%	(Walsh & Lindemann, 1984)
Water	Sawtooth	11%	Present study

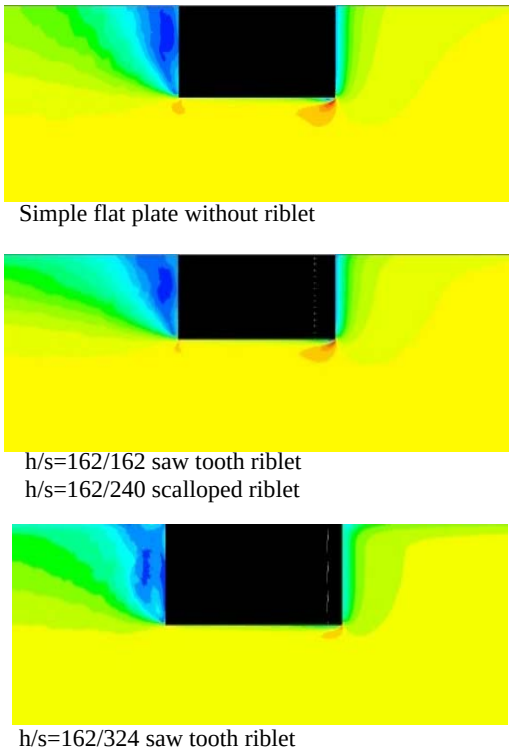

Simple flat plate without riblet

h/s=162/162 saw tooth riblet

h/s=162/240 scalloped riblet

h/s=162/324 saw tooth riblet

Fig. 13. Vortices status behind the flat plate having riblets of different size.

Figure 14 shows wake status at the back of flat plate with saw tooth riblets having two different dimensions. It shows that with *h/s*=1, more vortex are formed at the back of riblet flat plate and this can increase the drag on this flat plate.

5. Validation

In flight tests, total fuel consumption determines the amount of drag reduction. The 3M Corp (Minneapolis, MN) produces an experimental vinyl adhesive backed riblet sheet, which has been used in many fluid drag studies. The riblet cross sectional shape consists of equilateral triangles (saw tooth geometry) with *h/s*=0.5 (Marentic and Morris, 1992). The maximum drag reduction obtained from experiments performed by 3M riblets at different conditions together with the results of the present simulation are given in Table 2.

The results of series of simulations with *ANSYS CFX* were completely checked with the given results of former experiments. The modeled riblets were as the same size as the ones which were utilized in practice, and a good agreement were found.

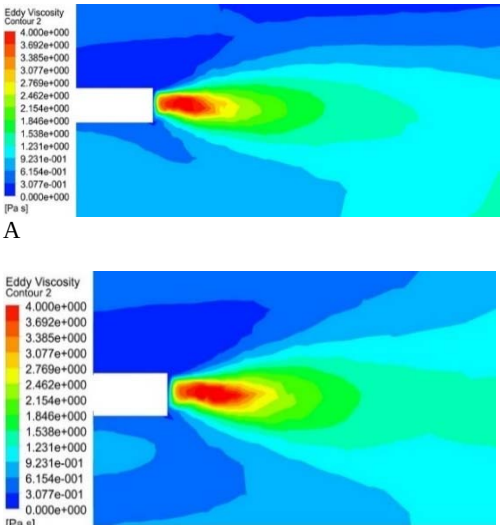

A

B

Fig. 14. Wake status at the back of flat plate with saw tooth riblet A:162/324, B:162/162.

6. CONCLUSIONS

This research numerically investigated the effects of shark's riblets on hydrodynamic parameters of submerged flat plate in water, for different types of riblets, *h/s* ratios and Reynolds numbers.

In this investigation, different types of riblets including sawtooth and scalloped riblets are simulated in *ANSYS CFX*. Results reveal that skin friction drag is efficiently reduced by the use of riblets through lifting turbulent vortices. Effects of transverse shear stress and momentum transfer are minimized by vortices lifting.

The highest drag reduction is attained with the riblets having smaller height. Less drag reduction is achieved with larger sized riblets, which sometimes

give even higher drag forces, compared to the simple plate. Experimental data obtained with the riblets of 3M Company were compared with the present numerical results. Based on the software results, saw tooth riblets have higher maximum drag reduction than scalloped riblets, but these riblets have lower lift extraction. Therefore, saw tooth riblets are suitable for water and air fluids, because in ships and aircrafts, the dominated force is drag force and saw tooth riblets can provide higher drag reduction than other types of riblets. By comparing the drag coefficients of simple and riblet flat plates it is concluded that riblets can reduce drag force about 11% and increase lift force about 6 %. A drag reduction up to 11% is technically feasible with an optimum riblet geometry and with a riblet aspect ratio of approximately h/s=0.5 for saw tooth riblets and h/s=0.7 for scalloped riblets, and it was shown that saw tooth riblet is the best type of riblets for drag reduction purposes.

REFERENCES

ANSYS CFX-Solver Theory Guide. (2011).

Bechert, D., M. Bruse, W. Hage, R. Meyer, D. Bechert, M. Bruse and R. Meyer (1997). Biological surfaces and their technological application - Laboratory and flight experiments on drag reduction and separation control *28th Fluid Dynamics Conference*: American Institute of Aeronautics and Astronautics.

Bechert, D. W., M. Bruse, W. Hage, J. G. T. Van Der Hoeven and G. Hoppe (1997). Experiments on drag-reducing surfaces and their optimization with an adjustable geometry. *Journal of Fluid Mechanics 338*, 59-87.

Bechert, W. D., M. Bruse and W. Hage (2000). Experiments with three-dimensional riblets as an idealized model of shark skin. *Experiments in Fluids 28*(5), 403-412.

Bhushan, B. (2012). Shark skin Surface for Fluid-Drag Reduction in Turbulent Flow. In B. Bhushan (Ed.), *Biomimetics: Bioinspired Hierarchical-Structured Surfaces for Green Science and Technology* (pp. 227-265). Berlin, Heidelberg: Springer Berlin Heidelberg.

Bixler, G. D. and B. Bhushan (2012). Biofouling: lessons from nature. *Philosophical Transactions of the Royal Society of London A: Mathematical, Physical and Engineering Sciences, 370*(1967), 2381-2417. Retrieved from abstract

Brian Dean, B. B. (2012). Shark-Skin Surfaces For Fluid-Drag Reduction In Turbulent Flow: A REVIEW. *Advances in Mechanics 42*(6), 821-836.

Brown, G. L. and A. Roshko (1974). On density effects and large structure in turbulent mixing layers. *Journal of Fluid Mechanics, 64*(04), 775-816.

Carman, M. L., T. G. Estes, A. W. Feinberg, J. F.Schumacher, W.Wilkerson, L. H. Wilson and A. B. Brennan (2006). Engineered antifouling microtopographies – correlating wettability with cell attachment. *Biofouling, 22*(1), 11-21.

Choi, K. S., X. Yang, B. R. Clayton, E. J. Glover, M. Atlar, B. N. Semenov and V. M. Kulik (1997). Turbulent drag reduction using compliant surfaces. *Proceedings of the Royal Society of London A: Mathematical, Physical and Engineering Sciences, 453*(1965), 2229-2240. Retrieved from abstract

Davies, C. and P. W. Carpenter (1997a). Instabilities in a plane channel flow between compliant walls. *Journal of Fluid Mechanics 352*, 205-243.

Davies, C. and P. W. Carpenter (1997b). Numerical simulation of the evolution of Tollmienand#8211;Schlichting waves over finite compliant panels. *Journal of Fluid Mechanics 335*, 361-392.

Dean, B. and B. Bhushan (2010). Shark-skin surfaces for fluid-drag reduction in turbulent flow: a review. *Philosophical Transactions of the Royal Society of London A: Mathematical, Physical and Engineering Sciences, 368*(1929), 4775-4806. Retrieved from abstract.

Fu, Y. F., C. Q. Yuan and X. Q. Bai (2017, 2017/03/01/). *Marine drag reduction of shark skin inspired riblet surfaces*. Biosurface and Biotribology (3, 1).

Fuaad, P. A., M. F. Baig and H. Ahmad (2016). Drag-reduction in buoyant and neutrally-buoyant turbulent flows over super-hydrophobic surfaces in transverse orientation. *International Journal of Heat and Mass Transfer, 93*(Supplement C), 1020-1033.

Goldstein, D., R. Handler and L. Sirovich (1995). Direct numerical simulation of turbulent flow over a modeled riblet covered surface. *Journal of Fluid Mechanics 302*, 333-376.

Hoyt, J. W. (1975). Hydrodynamic Drag Reduction Due to Fish Slimes. In T. Y. T. Wu, C. J. Brokaw and C. Brennen (Eds.), *Swimming and Flying in Nature: Volume 2* (pp. 653-672). Boston, MA: Springer US.

Krieger, K. (2004). Do Pool Sharks Swim Faster? *Science, 305*(5684), 636-637. Retrieved from abstract.

Lee, S. J. and S. H. Lee (2001). Flow field analysis of a turbulent boundary layer over a riblet surface. *Experiments in Fluids 30*(2), 153-166.

Matin, A., N. Merah and A. Ibrahim (2016). Superhydrophobic and self-cleaning surfaces prepared from a commercial silane using a single-step drop-coating method. *Progress in Organic Coatings, 99*(Supplement C), 322-329.

Shelley, S. R., J. D. Smith, A. P. Hibbins, J. R. Sambles and S. A. R. Horsley (2016). Fluid mobility over corrugated surfaces in the Stokes regime. *Physics of Fluids, 28*(8), 083101.

Shephard, K. L. (1994). Functions for fish mucus. *Reviews in Fish Biology and Fisheries 4*(4), 401-429.

Walsh, M., and A. Lindemann (1984). *Optimization and application of riblets for turbulent drag reduction*. 22nd Aerospace Sciences Meeting: American Institute of Aeronautics and Astronautics, Reno, NV,U.S.A

Zhao, D., Q. Tian, M. Wang and Y. Jin (2014). Study on the Hydrophobic Property of Shark-Skin-Inspired Micro-Riblets. *Journal of Bionic Engineering, 11*(2), 296-302.